Capillary Wave Dynamics of Thin Polymer Films over Submerged Nanostructures

K. J. Alvine,[1,2,*] Y. Dai,[3] H. W. Ro,[2] S. Narayanan,[4] A. R. Sandy,[4] C. L. Soles,[2,†] and O. G. Shpyrko[3,‡]

[1]*Energy and Environment Directorate, Pacific Northwest National Laboratory, Richland, Washington, 99352, USA*
[2]*Polymers Division, National Institute of Standards and Technology, Gaithersburg, Maryland 20878, USA*
[3]*Department of Physics, University of California, San Diego, La Jolla, California 92093, USA*
[4]*X-Ray Science Division, Argonne National Laboratory, Argonne, Illinois 60439, USA*

(Received 6 April 2012; published 13 November 2012)

The surface dynamics of thin molten polystyrene films supported by nanoscale periodic silicon line-space gratings were investigated with x-ray photon correlation spectroscopy. Surface dynamics over these nanostructures exhibit high directional anisotropy above certain length scales, as compared to surface dynamics over flat substrates. A cutoff length scale in the dynamics perpendicular to the grooves is observed. This marks a transition from standard over-damped capillary wave behavior to suppressed dynamics due to substrate interactions.

DOI: 10.1103/PhysRevLett.109.207801 PACS numbers: 61.25.H−, 62.23.St, 68.03.Kn, 68.15.+e

The behavior of soft matter and liquids over surfaces with nanoscale topography is an important area of active investigation in condensed matter physics and biology, with relevance to wetting phenomena [1,2], dewetting [3,4], self-assembly [5,6], and cellular adhesion [7,8]. The nanoscale surface topography strongly influences thin film wetting and morphology due to a confluence of van der Waals (vdW) interactions and surface tension effects. Examples include the wetting on complete [9] or partial nanoscale capillaries [1]. Furthermore, thermal liquid surface fluctuations (capillary waves) [10,11] can lead to film rupture and dewetting with unique patterns and morphologies [3,4,12,13]. The physics of liquid surface dynamics are of special interest in ultrathin polymer melts under vertical confinement where thicknesses approach the radius of gyration, R_g, of the macromolecule and suppression (slowing) of dynamics due to viscoelastic effects occurs [14]. Such confinement can alter film wetting behavior [4].

Surface dynamics of molten flat, uniform-thickness supported polymer films above the glass-transition temperature, T_g, have been extensively studied [14–17]. For molten polymer films, thick compared to the polymer radius of gyration R_g, the isotropic surface dynamics agree well with over-damped thermal capillary wave theory [15,18]. For ultrathin molten polymer films, with thickness 1–3 times R_g, viscoelastic effects suppress surface dynamics; when the thickness reaches R_g, no dynamics are observed [14]. In the present study, we investigate surface dynamics in a more complex thin polymer film system with laterally anisotropic thickness defined by a nearly flat polymer-air interface and a Si nanoscale line-space grating substrate (see Fig. 1). To the authors' knowledge, this is the first time surface dynamics have been investigated in such a system, though wetting in similar systems has been previously studied [1,2,19,20]. This novel system makes possible investigation of dynamics across ultrathin regions where viscoelastic effects are paramount. Our system includes ultrathin regions ($\sim 3R_g$) over the grating lines, where one expects viscoelastic and confinement effects, and thicker, bulklike (well above $4R_g$) regions, where confinement effects are expected to be negligible [14], and vdW substrate interactions and surface tension forces together induce an intrinsic periodic curvature to the polymer film that is quasiconformal to the underlying nanoscale grating [2,19]. X-ray photon correlation spectroscopy (XPCS) [21] was used to measure the wave vector dependence of the relaxation time for the capillary wave surface dynamics, quantifying dynamics in directions parallel and perpendicular to the long axis of the grating substructures over a range of temperatures well above the PS T_g. The resulting capillary wave dynamics are dramatically different in the two orthogonal directions. Parallel to the channel direction, our results can be described by the simple capillary wave model for flat isotropic films [15,18] using an effective film thickness as described below. In the perpendicular direction, however, we observed a characteristic length scale above which surface dynamics are strongly suppressed. This cutoff appears to be related to the capillary cutoff wave vector where the surface tension and vdW components balance [11] and is remarkably larger than the periodicity of the underlying grating. This suggests that capillary waves may propagate through ultrathin regions, which show complete suppression in the flat film of the same thickness.

Samples were prepared by spin-coating solutions of 3.7% by mass loading of PS with $M_w = 97\,000$ g/mol and polydispersity index 1.05 (Scientific Polymer Products Inc. [22]) dispersed in toluene over etched line-space silicon diffraction gratings (Light Smyth) at 2000 rpm, 1620 rpm/s for 60 s. The corresponding PS R_g is 8.4 nm [14]. Immediately prior to spin-coating, gratings were cleaned with standard *RCA*1 and *RCA*2 processes [23]. AFM of the bare gratings reveal 112 nm

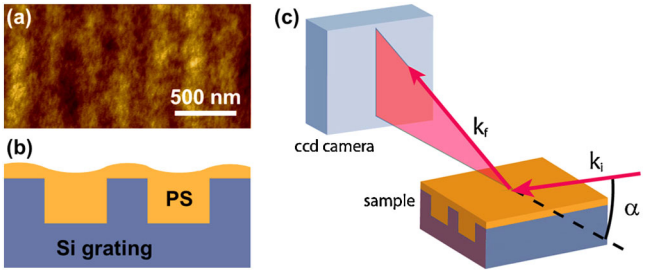

FIG. 1 (color online). (a) AFM image of the annealed PS film over the submerged nanoscale grating. "Hills" and "valleys" correspond to the lines and channels, respectively. (b) Cross-section illustration of the sample. (c) XRR and XPCS geometry. Note that for XPCS, the sample was measured in both perpendicular (shown) and parallel (sample rotated in-plane 90°) configurations.

tall lines with periodicity of 278 nm, a line-width of 129 nm, and a duty cycle of one. Spun-cast films on these gratings were then annealed under vacuum at 180 °C (well above the PS $T_g = 100$ °C) for 20 h to remove residual toluene and stress from the spin-casting process. AFM of the post-annealed sample [Fig. 1(a)] shows that the PS forms a continuous film without rupture over the nanoscale channels. Periodic height fluctuations of amplitude 1–2 nm in the PS film correlate with the periodicity of the underlying nanostructure and reflect a balance of vdW and surface tension forces [19]. A cross section is illustrated (with exaggerated curvature) in Fig. 1(b).

Room temperature x-ray reflectivity (XRR) measurements to extract the polymer film thickness profiles were performed at the 8-ID-I beam line of the Advanced Photon Source (APS), Argonne National Laboratory in the perpendicular configuration as shown in Fig. 1(c). The x-ray energy was 7.35 keV and a representative XRR profile from the sample is shown in Fig. 2(a). XRR is well suited for measuring nanoscale patterns [24] and buried interfaces providing the average electron density normal to the interface. Using the standard Parratt [25] formalism with a 3-layer model for electron density, combined with AFM data for linewidth and grating period, we extracted the film thickness profile from XRR fitting. The top two layers describe the PS above the nanoscale grating and the combination of polymer and grating, respectively. A third layer at the bottom of the channels, corresponding to bottom curvature of the channels, was required for good quality fitting. This bottom curvature was also observed with AFM and was likely an etching artifact. Slight deviations between the fit and the XRR data arise from nonzero sidewall angles and details of the curvature at the bottom of the channels that are not accounted for in the simple 3-layer model, which was primarily set up to determine PS film thickness across the sample. The resultant 3-layer model fit (normalized to the silicon electron density, ρ_∞) is shown in Fig. 2(b), with corresponding AFM data (averaged over several microns along the grating). The AFM line profile combines measurements from the bare grating and the PS film illustrated in Fig. 1(b). For visual comparison, the AFM data were shifted in the z direction to align with the interfaces in the electron density profile. From XRR fitting, the PS film thickness over lines is approximately 21 ± 5 nm (All uncertainties denote $\pm 1\sigma$) and 130 ± 5 nm over the channels. From AFM, the root mean square roughness value is 0.3 nm and the height variation is 1–2 nm over the PS surface, with the larger XRR value of roughness due to variations in the PS film averaged over large areas not accounted for with local AFM measurements. Note that, as the coefficient of thermal expansion for PS is roughly $7.5 \times 10^{-4}/$°C and $5.5 \times 10^{-4}/$°C below and above T_g, respectively [26,27], we expect that these thickness values will expand by no more than 5% as the temperature is increased to 180 °C and thermal expansion will have a negligible effect on our interpretation of the dynamics. The capillary wave relaxation dynamics [14,28] were measured by XPCS on the 8-ID-I beam line of the APS, at 7.35 keV. Beam dimensions were defined with slits to be 20 μm × 20 μm, comparable to the x-ray coherent lengths of 7 and 200 μm in

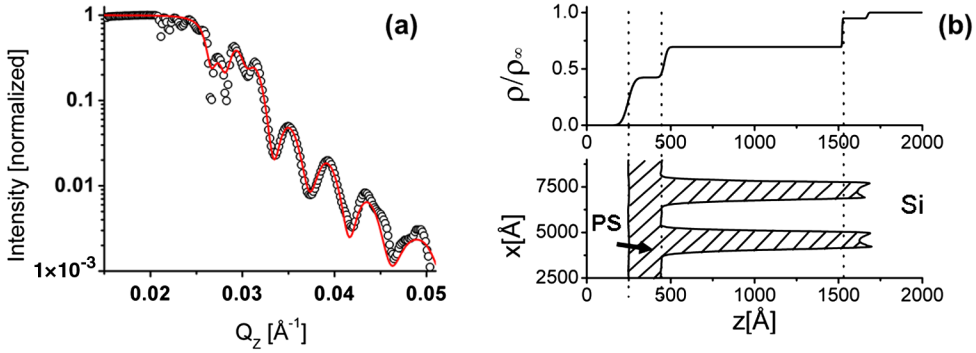

FIG. 2 (color online). (a) XRR data and fit (solid line) based on 3-layer model for the PS-grating combination. [(b), top] Electron density fit, normalized to Si. [(b), bottom] Corresponding AFM averaged line-profile data for the PS film (indicated by crosshatching) and the bare grating have been plotted on the same scale for comparison. AFM line profiles have been shifted along z, to align with the electron density profile.

the horizontal and vertical directions, respectively. The partially coherent x-ray beam scattered by the instantaneous arrangement of thermal capillary fluctuations produces "speckle" in the far-field scattering. By calculating the temporal autocorrelation function of the speckle intensities and fitting this with a single exponential decay function, we extracted the time-dependent relaxation of the capillary waves according to the procedure described in Refs. [15,29] with additional detail given in the Supplemental Material [30]. This single time-scale analysis represents the most straightforward approach to fitting the data. A more complex dual time-scale fitting analysis is described in [30]. XPCS measurements were performed at grazing angle with the x-ray beam either parallel or perpendicular to the grating lines as illustrated in Fig. 1(c). These are referred to as the parallel and perpendicular configurations, respectively. The grazing angle of 0.14° was below the PS critical angle, to ensure that XPCS measurements only probed the polymer surface with a penetration depth of 9 nm. Thus, x-ray speckle contrast results from height fluctuations at the polymer-air interface; static contributions from underlying Si topography are negligible [15]. Two-dimensional grazing incidence small angle x-ray scattering patterns were recorded on a 2D charge-coupled area detector 4 m downstream from the sample. Scattering over the wave vector Q range of 1×10^{-4} Å^{-1} to 1×10^{-3} Å^{-1} was collected with accessible time scales of 1 to 1000 s. XPCS data were collected under vacuum at sample temperatures between 140 °C and 180 °C where the PS behaves as a viscoelastic liquid.

The wave vector dependence of the capillary wave relaxation time scales are shown in Fig. 3(a) for the parallel configuration at 140 °C, 150 °C, 170 °C, and 180 °C. XPCS measurements in this parallel configuration are dominated by capillary wave dynamics along the channels, while perpendicular measurements are dominated by dynamics perpendicular to the channels. Cross-correlation between the parallel and perpendicular modes is not assumed in this analysis. In the parallel direction, relaxation times were fit [Fig. 3(a), solid lines] as a function of the in-plane wave vector Q, with the expression used for flat-film relaxations [15,18]:

$$\tau[Q] = \frac{2\eta[\cosh^2(Qh) + Q^2h^2]}{\gamma Q[\sinh(Qh)\cosh(Qh) - Qh]},$$

where η and γ are the bulk viscosity and surface tension, respectively. For this flat-film approximation, h represents an effective film thickness for the dynamics, which is affected by the relative interactions of the capillary waves with the channels. To determine h we assigned η/γ values interpolated from the literature for this molecular mass of PS as a function of temperature, leaving h as the only free fit parameter. From Refs. [26,31] the values of η/γ are approximately 4.3×10^{-2} s/nm, 7.8×10^{-3} s/nm, 5.9×10^{-4} s/nm, and 2.2×10^{-4} s/nm, for $T = 140$ °C, 150 °C, 170 °C, and 180 °C, respectively. Fit values for the effective thickness are then 168 ± 2 nm, 153 ± 3 nm, 141 ± 7 nm, and 104 ± 6 nm, respectively, for $T =$ 140 °C, 150 °C, 170 °C, and 180 °C. These effective film thickness values are of the same order of magnitude as the thickness measurements over the channel of 130 nm $\gg 4R_g$. At 140 °C, h is approximately 130% the maximum thickness, decreasing to 80% at 180 °C. This cannot be accounted for by polymer thermal expansion (5% at 180 °C, with the opposite trend), but may be due in part to the assumption of bulklike viscosity, as thin film confinement is known to affect this parameter [33]. Another issue arises from the first-order nature of our approximation of the nanostructured surface as an effective surface. The decrease in h with increasing temperature is indicative of a secondary effect. In particular, decreasing h may be caused by increased capillary wave amplitude and thus increased substrate interactions at elevated temperatures, leading to additional dynamics suppression at low Q.

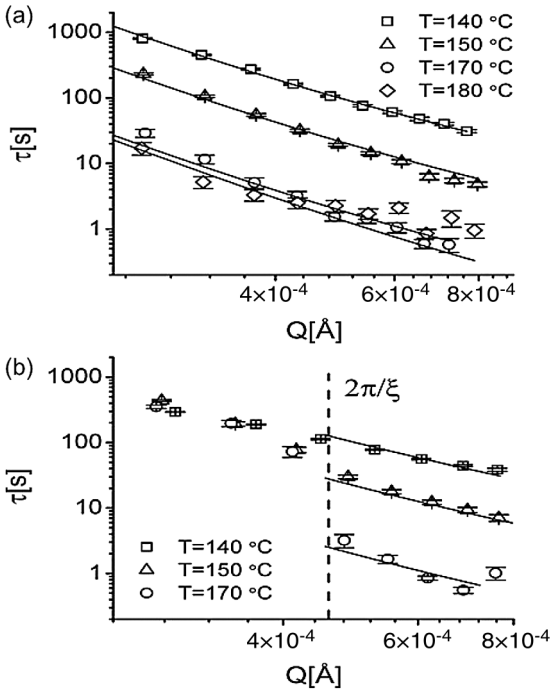

FIG. 3. (a) Capillary relaxation time constants as a function of wave vector Q for temperatures $T = 140$ °C, 150 °C, 170 °C, and 180 °C in the parallel configuration. Solid lines are fits to the data based on the flat-film model. (b) Capillary relaxation time constants for temperatures $T = 140$ °C, 150 °C, and 170 °C in the perpendicular configuration. Solid lines are the fit curves from the parallel data. The vertical dashed line represents the cutoff wave vector Q_c calculated in the text.

Relaxation time constants as a function of wave vector Q, measured in the perpendicular configuration, are shown in Fig. 3(b) for temperatures of 140 °C, 150 °C, and 170 °C. Data at 180 °C was not measured in this geometry due to the close similarity between the results observed in the parallel configuration between 170 °C and 180 °C.

In this configuration, XPCS probes dynamics propagating perpendicular to the channels, across the submerged corrugations. It is apparent from the data that the relaxation dynamics in the perpendicular configuration are radically different from those in the parallel configuration. A striking cutoff is observed for all temperatures at low Q. Fits (solid lines) from the parallel configuration data for the three temperatures are shown superimposed over the perpendicular data without modification, in the high Q range with good agreement. However, for low Q values below approximately 4.3×10^{-4} Å^{-1} (a length scale of $\sim 1.45\,\mu$m), the time scales for all temperatures superimpose and indicate dramatically suppressed dynamics. This transition is more pronounced at higher temperatures, though even the 140 °C data does not agree well with the "flat-film" model at the low-Q values. Moreover, the temperature dependence in the low Q range is negligible, indicating static or pinned behavior of the polymer. The low Q data cannot be fit well with the flat-film capillary wave model with any value of effective thickness. Since previous XPCS studies [14] have observed significantly suppressed dynamics in films with thickness 1–3R_g, we expect that dynamics at low Q (larger length-scales) are governed in part by regions over the lines where the thickness is 2–3R_g. When the film thicknesses drop below $2R_g$, chain confinement effects become important. The chains in such thin films are highly confined and have much greater surface interactions, similar to those of a grafted polymer brush [14,32]. In the case of grafted polymer brushes, long-wavelength ($\lambda \gg R_g$) fluctuations require relatively large lateral chain displacement to maintain monomer density and therefore have a high entropic penalty [34]. This penalty suppresses long-wavelength dynamics relative to R_g. A more complex treatment of the XPCS data for the perpendicular geometry using two time scales is given in the supplemental materials section. This alternate analysis suggests a possible combination of fast and slow dynamic behavior, where the slower dynamics dominate the behavior at low Q.

In our system, the nonuniform thickness introduces lateral anisotropy due to locally varying vertical confinement of the polymer. The nanoscale grating channel width is 129 nm, and yet we do not observe the transition to suppressed dynamics until much larger length-scales of 1.45 μm, which is roughly 5 periods of the underlying grating. This suggests that shorter wavelength modes may propagate across the ultrathin regions with thick-film-like dynamics. Otherwise, a transition length scale of approximately 129 nm should be observed. This adds new insight to previous studies [14] where all capillary wave dynamics were found to be significantly suppressed in ultrathin polymer films with thicknesses of 1–3R_g.

The interplay between surface tension and vdW polymer-substrate interactions may also contribute to the transition to suppressed dynamics along the perpendicular direction. This is evident by the sinusoidal surface undulations in the PS film measured with AFM and shown in Fig. 1(a). Surface tension acts to smooth or flatten the PS film, as there is an energetic penalty for film curvature, while the vdW polymer-substrate interactions act to make the film nearly conformal to the underlying structure [19]. Thus, the metastable [35] equilibrium state of the PS film over the submerged nanoscale grating is not flat, but has the weak surface corrugation correlating with the substrate. At small length scales and high Q, the surface tension dominates. At some value of $Q = Q_c$, however, there is a crossover to a vdW interaction dominated region at low Q. For $Q < Q_c$ the substrate interactions add additional penalty to surface height fluctuations. In the ultrathin region this Q_c corresponds to a cutoff length scale, $\xi = 2\pi/Q_c$, which is given by [11]

$$\xi = d^2\left(\frac{2\pi\gamma}{A_{\text{eff}}}\right)^{1/2},$$

where A_{eff} is the effective Hamaker constant for PS on silicon. The parameter d is the PS film thickness over the grating lines since the vdW effects from the channel bottoms are negligible [2]. Based on an effective Hamaker constant [36] $A_{\text{eff}} = 1.8 \times 10^{-20}$ J, surface tension $\gamma = 31$ mN/m, and film thickness of 21 nm over the lines, $\xi \approx 1.45$ μm which agrees remarkably well with the observed transition from fast to slow dynamics. The corresponding Q_c is denoted in Fig. 3(b) as a vertical dashed line. We point out that this is only a first-order approximation, and full analysis must include the system's periodic geometry. Nonetheless, this simple approximation elucidates fundamental physical behavior of the system.

We have used XPCS to investigate capillary wave dynamics of thin molten polymer films coated over submerged nanostructured gratings. This is a novel area of investigation where the vertical confinement is no longer uniform. The polymer film thickness over the tops of the grating lines is 2–3R_g, which is known to significantly suppress dynamics in the flat uniform-thickness films due to viscoelastic confinement effects [14]. Film thickness over the channel regions is considerably thicker, roughly 130 nm $\approx 16R_g$, where confinement effects and vdW substrate interactions are negligible. Capillary wave dynamics propagating parallel to the channels are in good agreement with the simple viscous film model, with an effective thickness close to the film depth over the channels. However, the capillary wave dynamics across the channels are dramatically different due to the combination of the PS film curvature and confinement effects arising from the vdW interactions with the substrate and the ultrathin nature of the PS film over the tops of the silicon lines. Below a cutoff length scale ($Q > Q_c$), dynamics are nearly identical to the parallel direction dynamics; above it, the dynamics are markedly suppressed and nearly temperature independent. The cutoff length-scale is remarkably well

represented by the crossover from surface tension dominated to vdW dominated interactions between the PS and the substrate. This value is several times the periodicity of the grating, indicating that capillary waves may propagate through ultrathin regions of the polymer film, which has not been observed previously. These observations may have important impact on the design of nanoscale topography for template dewetting [4] of nanoscale patterns and on the understanding of the ultrathin polymer film physics.

We thank W. Wu for valuable advice and thoughtful discussions. K. J. A. would like to acknowledge partial support from the NIST National Research Council. Partial support was also provided to K. J. A. by Pacific Northwest National Laboratory under DOE Contract No. DE-AC05-76RL01830. O. G. S. and Y. D. acknowledge support by the NSF CAREER Award Grant No. 0956131. Use of the APS was supported by the U.S. DOE, Office of Basic Energy Science, under Contract No. DE-AC02-06CH11357.

*kyle.alvine@pnnl.gov
†csoles@nist.gov
‡oshpyrko@physics.ucsd.edu

[1] O. Gang, K. J. Alvine, M. Fukuto, P. S. Pershan, C. T. Black, and B. M. Ocko, Phys. Rev. Lett. **95**, 217801 (2005).
[2] M. O. Robbins, D. Andelman, and J.-F. Joanny, Phys. Rev. A **43**, 4344 (1991).
[3] K. Y. Suh and H. H. Lee, J. Chem. Phys. **115**, 8204 (2001).
[4] K. Y. Suh, J. Park, and H. H. Lee, J. Chem. Phys. **116**, 7714 (2002).
[5] K. J. Alvine, D. Pontoni, O. G. Shpyrko, P. S. Pershan, D. J. Cookson, K. Shin, T. P. Russell, M. Brunnbauer, F. Stellacci, and O. Gang, Phys. Rev. B **73**, 125412 (2006).
[6] D. Pontoni, K. J. Alvine, A. Checco, O. Gang, B. M. Ocko, and P. S. Pershan, Phys. Rev. Lett. **102**, 016101 (2009).
[7] E. K. F. Yim, R. M. Reano, S. W. Pang, A. F. Yee, C. S. Chen, and K. W. Leong, Biomaterials **26**, 5405 (2005).
[8] S. D. Puckett, E. Taylor, T. Raimondo, and T. J. Webster, Biomaterials **31**, 706 (2010).
[9] K. J. Alvine, O. G. Shpyrko, P. S. Pershan, K. Shin, and T. P. Russell, Phys. Rev. Lett. **97**, 175503 (2006).
[10] A. Braslau, P. S. Pershan, G. Swislow, B. M. Ocko, and J. Als-Nielsen, Phys. Rev. A **38**, 2457 (1988).
[11] F. B. Wyart and J. Daillant, Can. J. Phys. **68**, 1084 (1990).
[12] K. J. Alvine, Y. F. Ding, J. F. Douglas, H. Ro, B. C. Okerberg, A. Karim, K. A. Lavery, S. Lin-Gibson, and C. L. Soles, Soft Matter **5**, 2913 (2009).
[13] K. J. Alvine, Y. F. Ding, J. F. Douglas, H. W. Ro, B. C. Okerberg, A. Karim, K. A. Lavery, S. Lin-Gibson, and C. L. Soles, J. Polym. Sci., Part B: Polym. Phys. **47**, 2591 (2009).
[14] Z. Jiang *et al.*, Phys. Rev. Lett. **98**, 227801 (2007).
[15] H. Kim, A. Ruhm, L. B. Lurio, J. K. Basu, J. Lal, D. Lumma, S. G. J. Mochrie, and S. K. Sinha, Phys. Rev. Lett. **90**, 068302 (2003).
[16] H. Kim, A. Ruhm, L. B. Lurio, J. K. Basu, J. Lal, S. G. J. Mochrie, and S. K. Sinha, J. Phys. Condens. Matter **16**, S3491 (2004).
[17] H. Kim, A. Ruhm, L. B. Lurio, J. K. Basu, J. Lal, S. G. J. Mochrie, and S. K. Sinha, Physica (Amsterdam) **336B**, 173 (2003).
[18] J. Jackle, J. Phys. Condens. Matter **10**, 7121 (1998).
[19] M. Tolan, G. Vacca, J. Wang, S. K. Sinha, Z. Li, M. H. Rafailovich, J. Sokolov, A. Gibaud, H. Lorenz, and J. P. Kotthaus, Physica (Amsterdam) **221B**, 53 (1996).
[20] I. M. Tidswell, T. A. Rabedeau, P. S. Pershan, and S. D. Kosowsky, Phys. Rev. Lett. **66**, 2108 (1991).
[21] S. G. J. Mochrie, A. M. Mayes, A. R. Sandy, M. Sutton, S. Brauer, G. B. Stephenson, D. L. Abernathy, and G. Grübel, Phys. Rev. Lett. **78**, 1275 (1997).
[22] Certain materials are identified in this Letter in order to adequately specify experimental details. Such identification does not imply recommendation by NIST, nor does it imply the materials are necessarily the best available for the purpose.
[23] W. Kern, *Handbook of Semiconductor Wafer Cleaning Technology: Science, Technology, and Applications* (Noyes Publications, Park Ridge, N.J., 1993).
[24] H. J. Lee, C. L. Soles, H. W. Ro, R. L. Jones, E. K. Lin, W. L. Wu, and D. R. Hines, Appl. Phys. Lett. **87**, 263111 (2005).
[25] L. G. Parratt, Phys. Rev. **95**, 359 (1954).
[26] J. I. E. H. Brandrup, *Polymer Handbook* (Wiley, New York, 1989), 3rd ed.
[27] W. J. Orts, J. H. van Zanten, W.-I. Wu, and S. K. Satija, Phys. Rev. Lett. **71**, 867 (1993).
[28] H. Y. Kim, A. Ruhm, L. B. Lurio, J. K. Basu, J. Lal, S. G. J. Mochrie, and S. K. Sinha, Mater. Sci. Eng., C **24**, 11 (2004).
[29] D. Lumma, L. B. Lurio, S. G. J. Mochrie, and M. Sutton, Rev. Sci. Instrum. **71**, 3274 (2000).
[30] See Supplemental Material at http://link.aps.org/supplemental/10.1103/PhysRevLett.109.207801 for information and example fits from an alternate dual time scale analysis of the data.
[31] J. C. Majeste, J. P. Montfort, A. Allal, and G. Marin, Rheol. Acta **37**, 486 (1998).
[32] B. Akgun, G. Ugur, Z. Jiang, S. Narayanan, S. Song, H. Lee, W. J. Brittain, H. Kim, S. K. Sinha, and M. D. Foster, Macromolecules, **42**, 737 (2009).
[33] C. L. Soles and Y. Ding, Science **322**, 689 (2008).
[34] G. H. Fredrickson, A. Ajdari, L. Leibler, and J. P. Carton, Macromolecules **25**, 2882 (1992).
[35] G. Reiter, Langmuir **9**, 1344 (1993).
[36] R. Seemann, S. Herminghaus, and K. Jacobs, Phys. Rev. Lett. **86**, 5534 (2001).